IET Microwaves, Antennas & Propagation

Research Article

IET Journals
The Institution of Engineering and Technology

Antenna development, link budget analysis and specific absorption rate evaluation in ultra-wideband implant communications

ISSN 1751-8725
Received on 4th January 2015
Revised on 23rd April 2015
Accepted on 19th June 2015
doi: 10.1049/iet-map.2014.0835
www.ietdl.org

Yuta Morimoto, Daisuke Anzai, Jianqing Wang ✉

Computer Science and Engineering, Nagoya Institute of Technology, Nagoya, Japan
✉ *E-mail: wang@nitech.ac.jp*

Abstract: In this study, the authors developed an ultra-wideband (UWB) planar loop antenna for implant communication, and confirmed its usefulness by comparing its designed and measured reflection and transmission characteristics. With the planar loop antenna as the implant transmitting antenna, then they calculated the implant path loss and specific absorption rate (SAR) using the finite difference time domain method together with an anatomical human body numerical model. Moreover, through a link budget analysis based on the calculated path loss with selection diversity, they derived the transmitting power required to achieve a specific bit error rate performance, and clarified the corresponding local SAR with respect to the international safety limits. As a result, the UWB implant communication is found to be feasible at a data rate as high as 40 Mbps under the SAR safety limits.

1 Introduction

In recent years, various efforts towards the realisation of a body area network (BAN) have been activating [1, 2]. BAN is usually used to collect biomedical information for medical diagnosis and health care monitoring. BAN is classified as wearable BAN and implant BAN. The wearable BAN monitors human's healthy conditions using wearable sensors, such as wearable electrocardiograph, while the implant BAN collects biomedical information using swallowed or implanted sensors. One of the typical examples of implant BAN is capsule endoscope. A capsule endoscope consists of a camera, a battery, a transmitter, and an antenna in dimensions of about 10 mm × 20 mm. It takes images of internal organs and transmits those to external devices for medical diagnosis. The current wireless communication systems for capsule endoscope mainly use the medical implant communication service (MICS) band at around 400 MHz [3]. However, its data rate is not enough to a high-speed video transmission. Accordingly, ultra-wideband (UWB) exhibits a potential for realising the high-speed transmission in capsule endoscope application [4, 5].

UWB is suitable for high-speed and low-power transmission. However, a UWB signal is largely attenuated in a human body because of its very short wavelength. Although so, the UWB technology still has a sufficient possibility to be applied to implant communication with high gain transmitting/receiving antennas, spatial diversity reception, and higher transmitting power. That is to say, we may increase the transmitting power to improve the UWB communication distance in the human body. This is because that the radiated power outside the human body is very weak due to the large attenuation inside the human body so that it no doubt satisfies various emission limits. The only concern is therefore the safety limit to the human body, i.e. the specific absorption rate (SAR), which should not exceed 2 W/kg for public people and 10 W/kg for occupational people for any 10 g of human tissue [6].

In this study, we attempt to clarify the UWB performance in implant communication based on the above-mentioned SAR limits. First, we make design for three types of implant transmitting antennas and compare their basic performances. Then, based on the ease of fabrication, we choose a planar loop antenna structure, and confirm its usefulness by comparing simulated and measured reflection and transmission characteristics. With the validated planar loop UWB antenna as the implant transmitting antenna, we calculate the implant path loss and local SAR using the finite difference time domain (FDTD) method together with an anatomical human body numerical model. Furthermore, through a link budget analysis based on the calculated path loss with selection diversity, we derive the transmitting power required to achieve a specific bit error rate (BER) performance, and compare the corresponding local SAR with the safety limits. In such a way, the feasibility of the UWB implant communication for high-speed video transmission is demonstrated under the SAR safety limits.

2 Designing implant antenna

An implant UWB antenna requires the antenna reflection coefficient S_{11} at least −9.5 dB at its working frequency band, i.e. between 3.4 and 4.8 GHz, the UWB low band, for a reasonable impedance matching. The S_{11} of −9.5 dB corresponds to a voltage standing wave ratio of 2.0, which means that almost 90% power supplied from the transmitter is sent to the antenna as the input power [7]. So this value is often used as a design index of the antenna. It is also necessary to have a small size and light weight because the antenna has to match for a capsule endoscope. In view of the shape of the capsule, the first choice is to form the transmitting antenna on the hemisphere of the capsule [8]. The hemisphere is usually a dielectric material with a relative permittivity of 3 and a radius of 5 mm. Moreover, it is covered with polyethylene with a relative permittivity of 2.2 and a thickness of 0.1 mm. Since the transmitting antenna in the human body is affected by the dielectric properties of the surrounding human tissue, the actual wavelength in the human body is shorter than that in the free space. The relation between the wavelength in the free space and that of the human body is expressed as follows [2]

$$\lambda_{\text{eff}} = \frac{\lambda_0}{\text{Re}\left[\varepsilon_{\text{r}} - \text{j}\sigma/\omega\varepsilon_0\right]} \tag{1}$$

where λ_{eff} is the wavelength in the human body, λ_0 is the wavelength in the free space, ε_{r} and σ are the relative permittivity and conductivity of the human body, respectively, ω is the angular frequency, and ε_0 is the permittivity in the free space. The resonance frequency in the human body was roughly estimated to be about 1/4 of the free-space wavelength due to the reduction effect of the dielectric constants of the human body as well as the

hemisphere and the polyethylene capsule cover. Accordingly, this effect in the resonance frequency has to be taken into account for the design of implant antennas.

Fig. 1*a* shows a hemispherical helical antenna structure. Typically, a helical antenna operates at the axial mode on condition that a total antenna length is more than one wavelength. The characteristics of an axial mode helical antenna are its wide bandwidth and sharp directivity. The proposed hemispherical helical antenna was composed of a microstrip line of about three wavelengths to widen the bandwidth. The microstrip line with a width of 0.5 mm was wound three times onto the hemisphere at an interval of 1 mm. Fig. 1*b* shows another hemispherical antenna structure in a loop shape. The proposed loop antenna had a wide element to widen its bandwidth. The element had an inner radius of 3.1 mm and an outer radius of 3.5 mm. The total length of the inner loop was one wavelength of the resonance frequency. The feeding part had an angle of 45° to reduce the reactance component. This antenna operated as a one-wavelength loop antenna which radiates towards the *z*-axis direction.

The two hemispherical antennas were placed in a homogeneous rectangular torso model with average dielectric properties of muscle tissue, respectively, for performance evaluation. The relative permittivity of the human tissue increases with frequency, and the conductivity of the human tissue decreases with frequency. This frequency dependence was taken into account in the FDTD simulations [9]. Fig. 1*c* shows the FDTD-simulated S_{11} performances for the two kinds of hemispherical antennas. Both antennas exhibit an S_{11} performance smaller than −10 dB in the UWB low band, and the loop antenna has a better S_{11} performance. Fig. 2 shows the directivity of the two hemispherical antennas in the homogeneous torso model at the centre frequency of 4.1 GHz. Both antennas give a flat directivity in the *xy*-plane. In the *yz*-plane, the helical antenna seems more flat in the directivity, but it has no obvious advantage. In view of the above simulation results and the consideration on ease of fabrication, we decided to choose the loop antenna as the implant transmitting antenna.

To simplify the antenna fabrication, instead of the hemispherical antenna structure, we further investigated the possibility of a planar structure for the wideband loop antenna. The planar loop

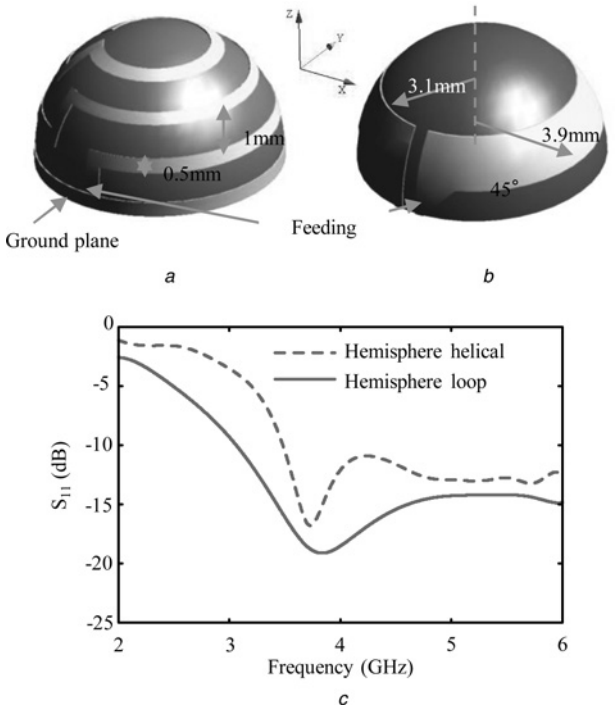

Fig. 1 *Hemispherical antenna structure*

a Hemispherical helical antenna structure
b Hemispherical loop antenna structure
c Simulated S_{11} performances for the two hemispherical antennas

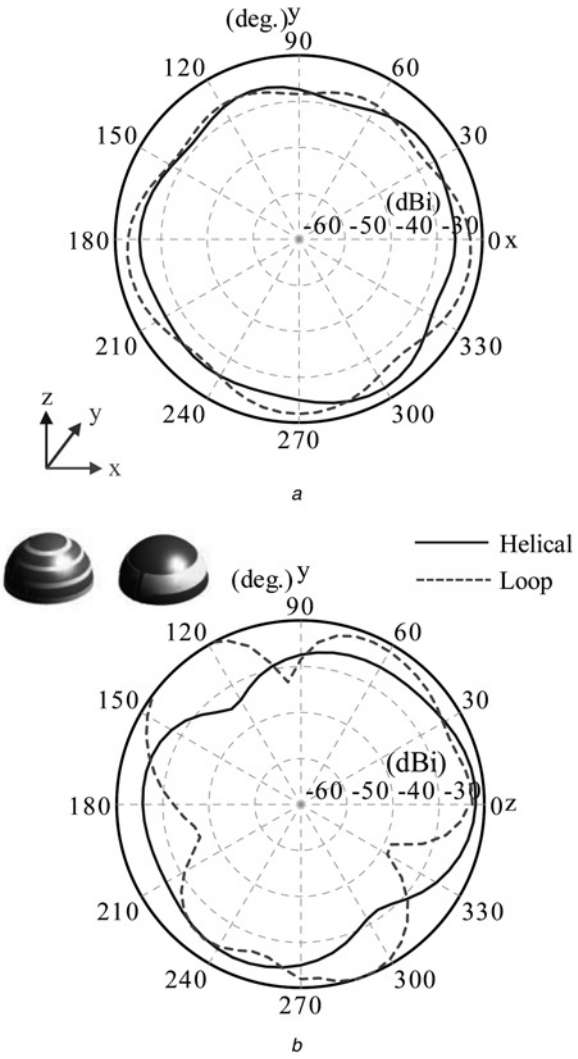

Fig. 2 *Directivity of the two hemispherical antennas in a homogeneous torso model at 4.1 GHz*

a X-Y plane (4.1 GHZ)
b Y-Z plane (4.1 GHZ)

antenna was a modified one of the hemispherical loop antenna. Fig. 3*a* shows the planar loop antenna structure. The microstrip line with a width of 1 mm was built on a planar substance with a relative permittivity of 4 and a thickness of 1.6 mm. The loop radius was 4 mm. Since an implant antenna usually does not directly touch with a human body tissue, a thin plastic layer was arranged around the planar loop antenna. This antenna also operated as a one-wavelength loop antenna which radiates towards the *z*-axis direction in the human body. The S_{11} and S_{21} performances and the directivity of the planar loop antenna in the UWB low band were simulated in a homogeneous torso model by the FDTD method, and the simulated results were compared with measured ones to confirm the validity. Fig. 3*b* shows the setup for S_{11} and S_{21} measurements. In the measurement, the planar loop antenna was located in a liquid phantom which had dimensions of 28 cm × 16 cm × 22 cm. The dielectric properties of the liquid phantom were measured with a dielectric probe kit (Agilent, 85070), and Table 1 gives the measured values at several specific frequencies. The liquid phantom was used to simulate an average dielectric property of the human body. The average dielectric property of the human body is known to be nearly the 2/3 value of muscle tissue. As shown in Table 1, the measured results show that the relative permittivity of the liquid phantom was the almost same as the 2/3-muscle value, but the conductivity was somewhat higher than the 2/3-muscle value. Fig. 4 shows the simulated and the measured S_{11} for the planar loop antenna. Also shown in

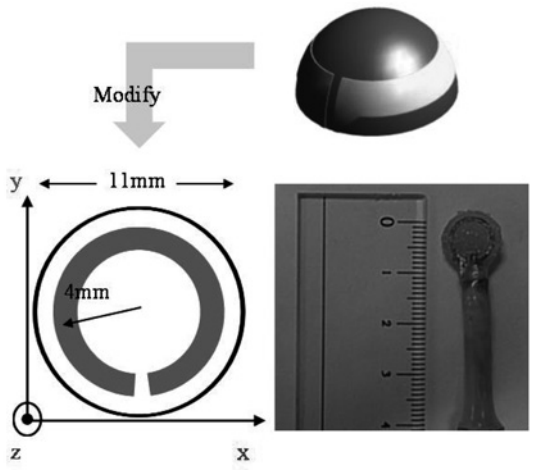

Fig. 3 *Planar loop antenna structure*

a Modified planar loop antenna structure
b Setup for S_{11} and S_{21} measurements

Fig. 4 is the simulated S_{11} for the hemispherical loop antenna. As can be seen, the planar loop antenna provides an S_{11} performance similar to the hemispherical loop antenna, and the fabricated one exhibits a measured S_{11} smaller than −10 dB in the UWB low band. The measured S_{11} agrees fairly with the simulation, and the difference of the resonant frequency between the measurement and simulation should be attributed to the fabrication uncertainty especially in the SMA adaptor part. If we want to further broaden the bandwidth of the loop antenna, a feasible method is to use wider cooper wire as the loop element. In addition, Fig. 5 shows the simulated directivity of the planar loop antenna at 3.4, 4.1, and 4.8 GHz in the liquid phantom. It is found that the antenna exhibits a relative flat directivity in both the *xy*-plane and the *yz*-plane, and the differences among different frequencies are insignificant. Although the nulls in some specific directions seem more obvious at higher frequencies, they are not smaller than 22 dB compared to the maximum radiation. Since there is no very sharp null in the both planes, the antenna directivity of the planar loop antenna is suitable for the capsule endoscope application in which the capsule continues to change its position and direction.

Table 1 Dielectric properties of the liquid phantom

Frequency, GHz	Relative permittivity	Conductivity, S/m
3.4	38.2	2.6
4.1	36.1	3.4
4.8	34.2	4.1

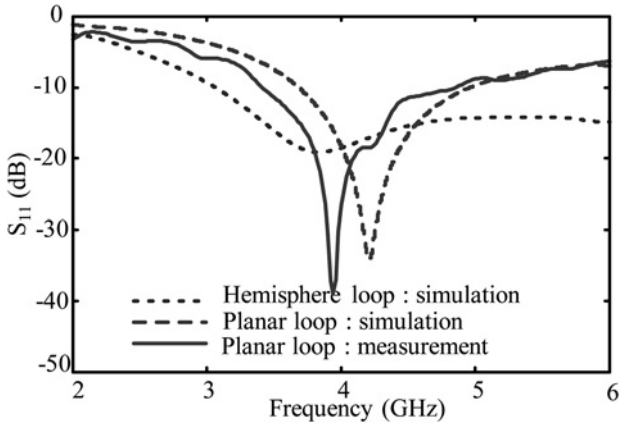

Fig. 4 *Simulated and measured S_{11} performances for the planar loop antenna*

Table 2 compares the same typed implant UWB antennas on key parameters, such as the −10 dB bandwidth, antenna gain, and dimensions. Our planar loop antenna has a lower profile or smaller dimensions than that in [10, 11], and a much simpler shape than that in [12]. Since the antenna gains were given at different situations, the results cannot be compared directly.

3 Propagation characteristics

3.1 S_{21} in liquid phantom

In order to realise a wireless link from the implant antenna to the outside of body, a planar unbalance dipole antenna was developed to operate as a receiving antenna on the body surface. Fig. 6*a* shows the fabricated planar unbalanced dipole antenna based on [13]. The antenna was built on the substance with a relative permittivity of 4 and a thickness of 1.6 mm, and had two different shaped elements to widen the bandwidth. From the point of views of antenna miniaturisation, a coaxial cable feeding is undesirable. Accordingly, the semi-circle was fed by a microstrip line and the trapezoid element was used as the ground. The electrical current concentrated on the edges of the antenna. Therefore, even if the microstrip line was placed in the centre of the trapezoid element, the radiation from the antenna was not affected significantly. This antenna was used on the surface of the liquid phantom with a spacing of 1 cm. The S_{11} performance was measured and shown in Fig. 6*b*, which exhibits an S_{11} smaller than −10 dB in the UWB low band.

Furthermore, the S_{21} performance was also simulated and measured in the arrangement in Fig. 7. As the transmitting antenna, the planar loop antenna was located in the liquid phantom under a 15-cm depth, while the planar unbalanced dipole antenna was located on the liquid phantom surface for reception. The major directivities were set to be identical between the planar loop transmitting antenna and the unbalanced dipole receiving antenna. With a network analyser, the S_{21} between the transmitting and receiving antennas was measured at the centre frequency of 4.1 GHz. As shown in Fig. 7, the measured S_{21} agrees well with the FDTD-simulated one, which assures the validity of the FDTD simulations. The slight difference at the distance smaller than 2 cm was considered to be due to the influence of the coaxial cable and adaptor. It was found that the propagation loss is about 70 dB at a depth of 5 cm from the phantom surface.

3.2 Path loss in anatomical human body model

In order to derive the actual path loss in a human body for our designed implant antenna, we employed an anatomical human body numerical model developed by National Institute of Information and Communication Technology, Japan [14]. It

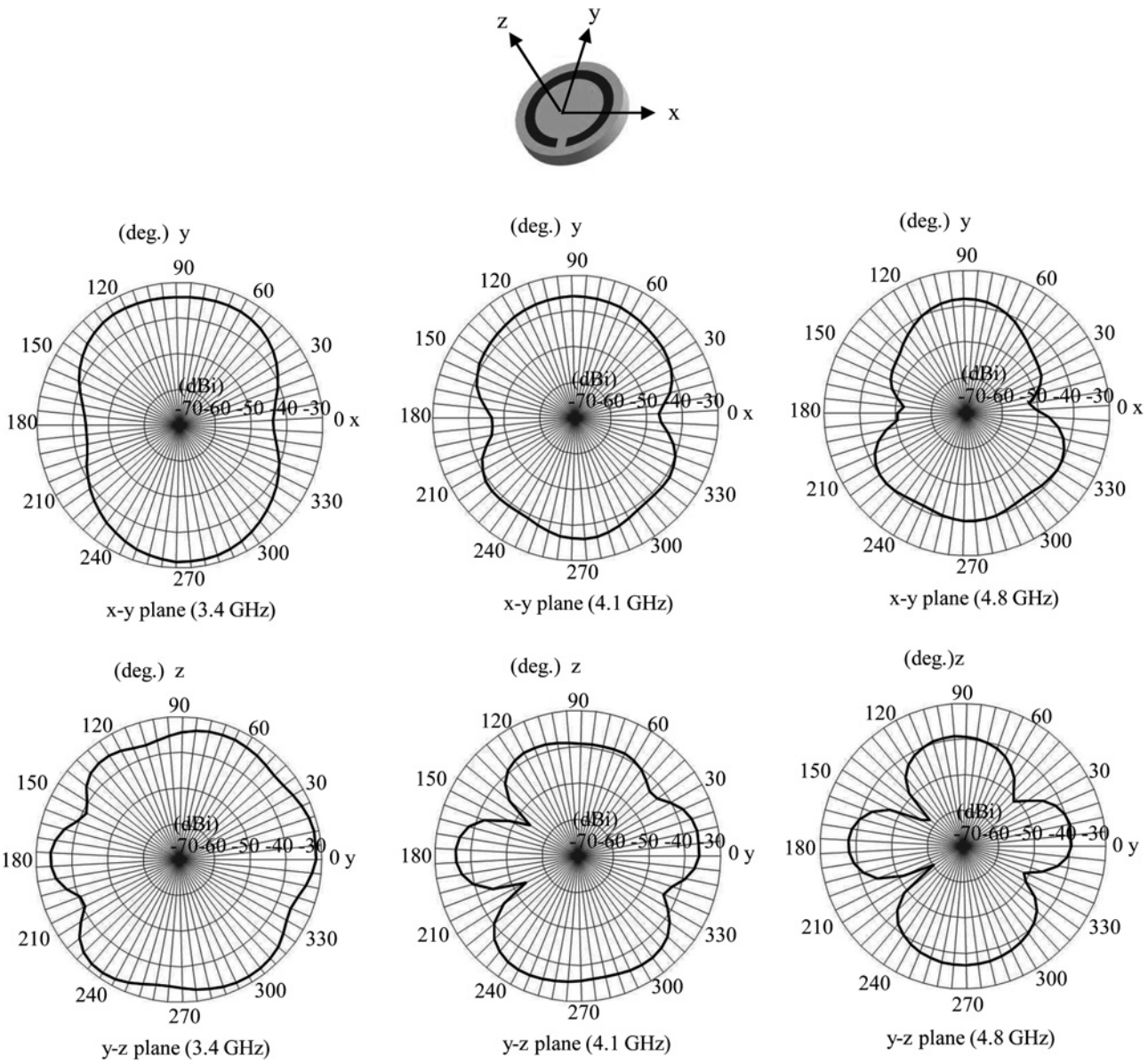

Fig. 5 *Directivity of the planar loop antenna in a liquid phantom at 3.4, 4.1, and 4.8 GHz*

consists of 51 tissue types and has a resolution of 2 mm. The planar loop antenna was set at 21 positions inside the small intestine, and took three possible directions along the x, y, or z axis. On the other hand, five planar unbalanced dipole receiving antennas were located around the abdominal region of the human body for diversity reception as shown in Fig. 8. The path loss between the transmitting and receiving antennas is then calculated as

$$\mathrm{PL}_{\mathrm{dB}} = 10\log_{10}\frac{P_{\mathrm{t}}}{P_{\mathrm{r}}} \tag{2}$$

where P_{t} and P_{r} are the transmitting power and receiving power, respectively, both calculated by the FDTD method. It should be noted that the path loss contains not only the attenuation in the human body but also the transmitting and receiving antenna gains. In order to cope with the large attenuation in the human body in a UWB low band, we assumed the employment of selective diversity which selects the minimum path loss among the five receiving antennas. Fig. 9 shows the FDTD-calculated path loss for the anatomical human body model with selection diversity. As can be seen from the figure, compared to the liquid phantom, the path loss was improved to be about 50 dB at the same distance of 5 cm. This improvement should be attributed the selection diversity reception. As a result of selection diversity, the average path loss is around 80 dB at 10 cm depth and 100 dB at 15 cm depth in an actual human body.

Table 2 Comparison of the same typed UWB implant antennas

Reference	Antenna type	−10 dB Bandwidth	Maximum gain at 4.1 GHz	Dimensions
Dissanayake *et al.* [10]	planar dipole with a grounded coplanar waveguide feed	3.5–4.5 GHz	2 dB in free space	$14 \times 14 \times 28.7$ mm^3
Wang *et al.* [11]	dielectric resonator antenna	3–5 GHz	−24 dB inside a $20 \times 20 \times 20$ cm^3 body	$8 \times 8 \times 4$ mm^3
Yazdandoost [12]	planar loop with a complex shape	3.1–10.6 GHz	−15 dB beneath skin	$10 \times 9 \times 0.5$ mm^3
our, 2015	planar circular loop	3.4–4.8 GHz	−34 dB inside a $28 \times 16 \times 22$ cm^3 body	$11 \times 11 \times 1.6$ mm^3

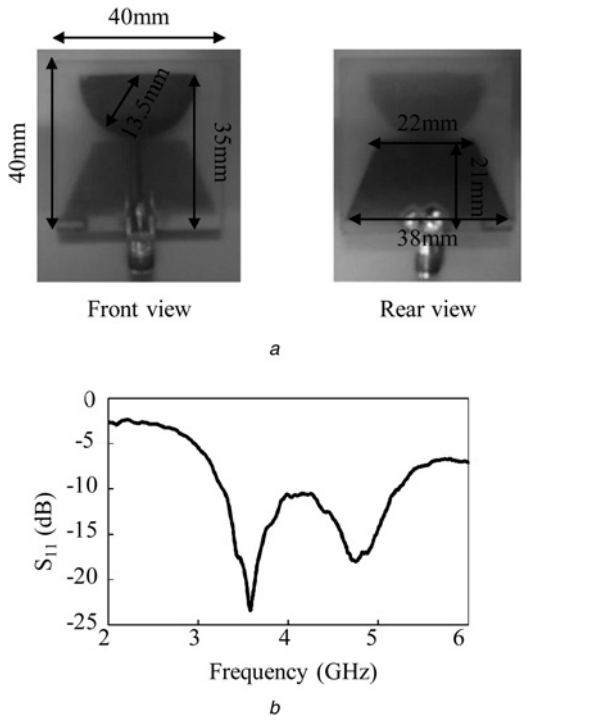

Fig. 6 *Fabricated planar unbalanced dipole antenna*

a Fabricated planar unbalanced receiving dipole antenna
b Measured S_{11} performance of the planar unbalanced receiving dipole antenna

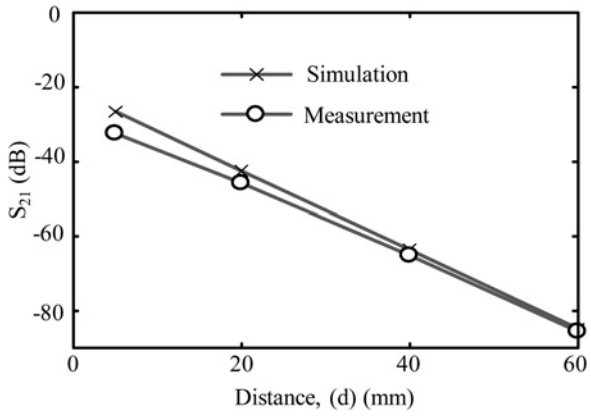

Fig. 7 *Simulated and measured S_{21} performance at 4.1 GHz*

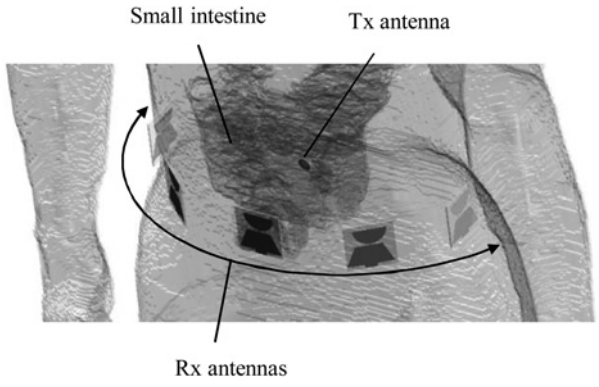

Fig. 8 *Human body model and arrangement of the implant transmitting antenna and five receiving antennas*

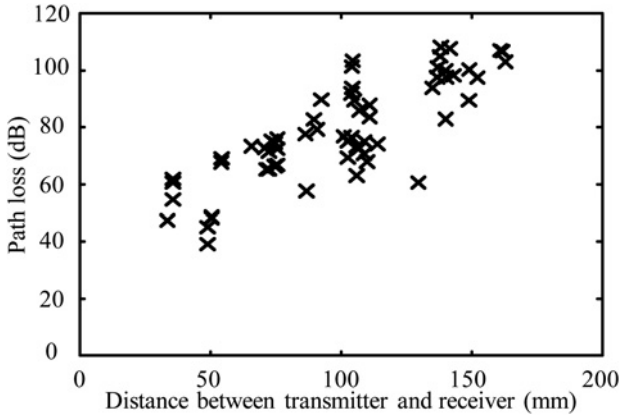

Fig. 9 *FDTD-calculated path loss in the anatomical human body model with selection diversity*

4 Transceiver and receiver structure

The required transmitting power for achieving a specified communication performance, i.e. BER, was calculated based on the above-derived path loss for the developed implant transmitting antenna and receiving antenna. A UWB impulse radio (IR) scheme with binary pulse-position modulation (PPM) was adopted in the modulator, in which the data bits were sent as position information of a UWB pulse [15]. When the total transmitted bits are K, the PPM signal waveform $s(t)$ can be expressed as

$$s(t) = \sum_{k=0}^{K} p\left(t - b_k \frac{T}{2} - kT\right) \tag{3}$$

where b_k is the kth transmitted bit, namely $b_k \in \{0,1\}$ ($k = 0, 1, \ldots, K$), and T is the symbol duration.

The receiver employed energy detection as the signal detection scheme. As shown in Fig. 10, after the front-end, such as low-noise amplifier and band-pass filter, two kinds of energies for the kth bit were calculated from the received signal $r(t)$ as

$$E_k^0 = \int_{kT}^{kT+T_d} [r(t)]^2 \mathrm{d}t \tag{4}$$

$$E_k^1 = \int_{\left(k+\frac{1}{2}\right)T}^{\left(k+\frac{1}{2}\right)T+T_d} [r(t)]^2 \mathrm{d}t \tag{5}$$

where T_d denotes the energy detection duration. By comparing E_k^0 and E_k^1, the received bit b_k can be decided as

$$\hat{b}_k = \begin{cases} 0, & \text{if} E_k^0 > E_k^1 \\ 1, & \text{otherwise} \end{cases}. \tag{6}$$

However, the receiver signal $r(t)$ contains a noise $n(t)$, which is a wideband noise because of the employed UWB-IR scheme. According to [16], a wideband signal can be approximated as M narrow band signals when M is sufficiently large, so that $2M \simeq 2BT_d$ where B is the bandwidth of the UWB-IR signal. Since each approximated narrow band noise is a zero mean independent Gaussian distribution with variance of $N_0/2$, the detected energy E_k^0 or E_k^1 is a sum of $2M$ independent variables with a chi-square distribution. Its probability distribution can be thus approximated as a Gaussian distribution according to the central limit theorem. When the UWB signal is not present in the detection time, the mean and the variance are MN_0 and MN_0^2, respectively. When the UWB signal is present with energy E, the mean and the variance are $MN_0 + E$ and $MN_0^2 + 2EN_0$, respectively. Based on the

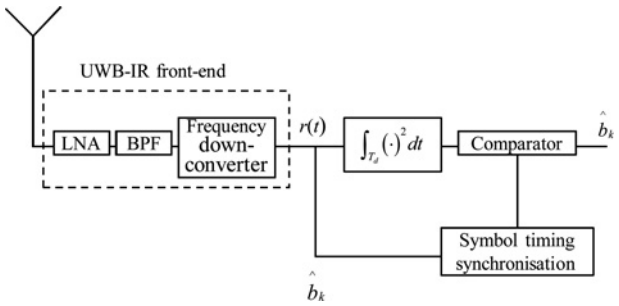

Fig. 10 *Receiver structure with energy detector*

Gaussian approximation, under the assumption that the outputs of the detector are E_1 and E_2 when the signal are present and absent, respectively, the BER P_e is given by [17]

$$P_e = \text{prob}(E_2 > E_1) = \int_{E_1=0}^{\infty} p(E_1)\left[\int_{E_2=E_1}^{\infty} p(E_2)\text{d}E_2\right]\text{d}E_1 \quad (7)$$

When the energy detection duration T_d is taken as the reciprocal of the frequency bandwidth, i.e. $1/B$, the BER P_e can be further approximated with the following formula

$$P_e = \frac{1}{2}\text{e}^{-E_b/2N_0} \quad (8)$$

where E_b is the energy per bit.

5 Quantitative relationship between required power and SAR

Communication performance is usually evaluated by the BER. BER $\leq 10^{-2}$ is considered to be acceptable in the physical layer because an error-free communication may be achieved by introducing a forward error correction technique at such a BER level. Therefore, we chose BER $= 10^{-2}$ as a required communication performance, and investigated the required transmitting power and SAR based on the above-derived path loss. From (8), it was found that an E_b/N_0 of 9 dB is required to get BER $= 10^{-2}$. By denoting f_b as the data rate and B as the bandwidth, the receiving power P_r can be expressed as

$$P_{r_{dBW}} = E_b/N_{0,dB} + 10\log_{10}\frac{f_b}{B} + N_{dBW}, \quad (9)$$

where $N = kTBN_F$ is the noise power, k is the Boltzmann constant, T is the environment temperature, and N_F is the noise figure of the front-end of receiver. Under the specifications listed in Table 3 for the UWB-IR system, the receiving power $P_{r,dBW}$ was calculated as -130 dBW for achieving a specified BER performance of 10^{-2}. With the calculated receiving power and the path loss at location d of the transmitting antenna inside the human body, the required transmitting power at the location d can be obtained as

$$P_{t,dBW}(d) = PL_{dB}(d) + P_{r,dBW} \quad (10)$$

It means that the required transmitting power is different at different locations inside the human body for achieving a specific BER performance, and thus the SAR is also different when the transmitting antenna locates at different locations. The SAR calculation was conducted at the same time of the path loss calculation by the FDTD method together with the anatomical human body model. Under the transmitting power obtained from

Table 3 Specifications of the communication system

Modulation	PPM
de-modulation	energy detection
data rate	1 Mbps
bandwidth	1.4 GHz
channel	additive white noise
temperature	300 K
front-end noise figure	6 dB

(10), the SAR is calculated from [18]

$$\text{SAR} = \frac{1}{T_b}\int_{3.4\text{GHz}}^{4.8\text{GHz}} \sigma(f)\left|E(f)\right|^2/\rho\,\text{d}f \quad (11)$$

where $\sigma(f)$ and ρ are the conductivity and mass density of human tissue, respectively, $E(f)$ is the Fourier transfer of the internal electric field $E(t)$, and $T_b = 1/f_b$ is the bit period. It should be emphasised that the SAR is dependent on the bit period, and the bit period is usually larger than the pulse duration. For a UWB low-band pulse between 3.4 and 4.8 GHz, its pulse duration is in the order of nanoseconds.

For a localised radio-frequency exposure, the 10 g-averaged spatial peak SAR is used as an index for safety evaluation in various international safety guidelines. ICNIRP suggests a safety limit of 2 W/kg for public people and 10 W/kg for occupational people for any 10 g-averaged spatial peak SAR [6]. From the SAR value calculated with (11) in each FDTD voxel, we derived the

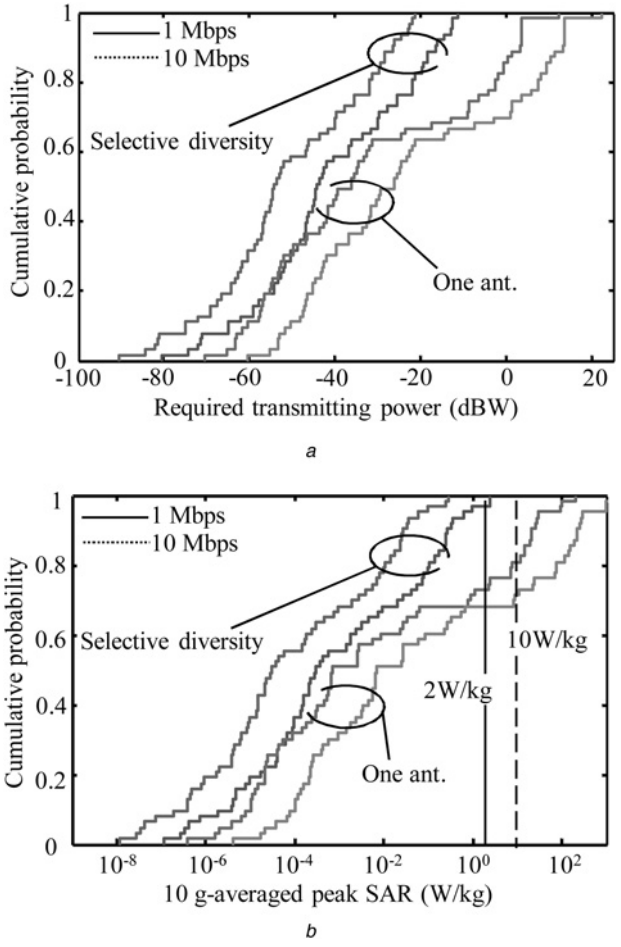

Fig. 11 *Cumulative distribution of the*

a Required transmitting powers in the small intestine for achieving a BER of 10^{-2}
b 10 g-averaged spatial peak SAR under the transmitting power required for achieving a BER of 10^{-2}

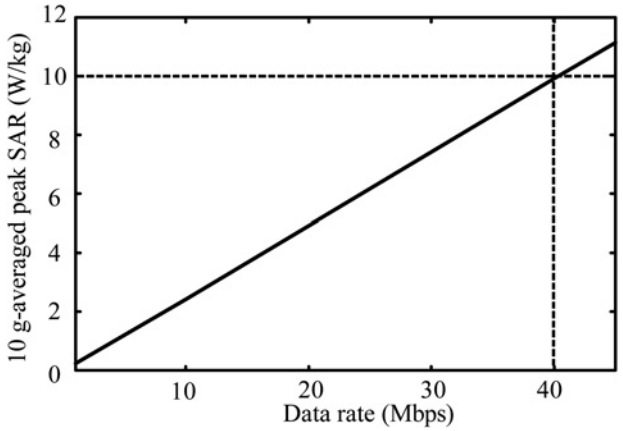

Fig. 12 *Maximum 10 g-averaged spatial peak SAR in the small intestine versus the data rate*

Table 4 Required transmitting power and 10 g-averaged SAR versus data rate

Data rate, Mbps	Required transmitting power, mW		10 g-averaged peak SAR, W/kg	
	Mean	Standard deviation	Mean	Standard deviation
1	0.655	1.575	0.0147	0.0474
10	6.628	16.051	0.1403	0.4397
40	26.678	64.151	0.5982	1.9343

10 g-averaged spatial peak SAR by averaging the voxel SARs within a cube weighing approximately 10 g.

Fig. 11*a* shows the cumulative distribution of the required transmitting powers at all the locations in the small intestine for achieving a BER of 10^{-2} at data rates of 1 and 10 Mbps, respectively. The required transmitting power is obviously dependent on the data rate, and a higher data rate requires more transmitting power in order to achieving the same BER performance. In addition, compared to the required transmitting power in the case of one receiving antenna, the selective diversity reception significantly reduces the required transmitting power. For example, at nearly 90% capsule locations, the one receiving antenna requires a transmitting power of 13 dBW at maximum at 10 Mbps, while the selection diversity makes the required transmitting power reduce to −17 dBW at maximum, which means a reduction effect of 30 dB.

Fig. 11*b* shows the 10 g-averaged spatial peak SAR under the transmitting power required for achieving a BER of 10^{-2}. As the data rate increases, the required transmitting power will increase as can be seen from (9). The increased transmitting power yields more energy absorbed by the human body, and the SAR is further increased by the shortened bit period T_b. It can be found that the 10 g-averaged spatial peak SAR will never exceed the safety limit of 2 W/kg at 1 Mbps and 10 W/kg at 10 Mbps with selection diversity reception. In addition, compared to one antenna reception, the selective diversity reception significantly reduces the 10 g-averaged spatial peak SAR by a factor of around 20 at an average. To further clarify the possible maximum data rate under the SAR safety limits, we also show the maximum 10 g-averaged spatial peak SAR in the small intestine as a function of data rate in Fig. 12. From the figure, it can be confirmed that our UWB-IR system can provide a reliable implant communication, i.e. at a BER of 10^{-2}, at a data rate up to 40 Mbps under the SAR safety limits. Table 4 summarises the mean and standard deviation of the required power and 10 g-averaged peak SAR for all considered locations in the small intestine with selection diversity reception.

6 Conclusion

The feasibility of UWB implant communication has been investigated in this study. At first, we designed three types of implant transmitting antennas and compared their basic performances. Based on the comparison and the ease of fabrication, we have determined to choose a planar loop antenna structure in the implant transmitter, and have confirmed its usefulness through comparison of simulated and measured antenna reflection and transmission characteristics. Although the planar loop antenna exhibits a little lower antenna gain compared to the hemispherical antennas, it is available to be improved by employing a dielectric substrate with lower permittivity. With the validated planar loop UWB antenna, we have calculated the implant path loss and SAR using the FDTD method together with an anatomical human body numerical model. Through a link budget analysis based on the calculated path loss with selection diversity reception, we have derived the cumulative distribution of the transmitting power required for achieving BER = 10^{-2} and clarified the corresponding 10 g-averaged spatial peak SARs under the required transmitting powers. The results have shown the feasibility of UWB implant communication at a data rate as high as 40 Mbps under the ICNIRP SAR safety limits of 10 W/kg for any 10 g of tissues.

One of the future subjects is to develop an algorithm to effectively control the transmitting power based on the received signal levels in order to make the localised SAR as low as possible.

7 References

1 Astrin, A.W., Li, H.-B., Kohno, R.: 'Standardization for body area networks', *IEIEC Trans. Commun.*, 2009, **E92-B**, (2), pp. 366–372
2 Wang, J., Wang, Q.: 'Body area communications' (Wiley-IEEE, 2013)
3 Yuce, M.R., Dissanyake, T.: 'Easy-to-swallow wireless telemetry', *IEEE Microw. Mag.*, **13**, (6), 2012, pp. 99–101
4 Chavez-Santiago, R., Sayrafian-Pour, K., Khaleghi, A., *et al.*: 'Propagation models for IEEE 802.15.6 standardization of implant communication in body area networks', *IEEE Commun. Mag.*, 2013, **51**, (8), pp. 80–87
5 Anzai, D., Katsu, K., Chavez-Santiago, R., *et al.*: 'Experimental evaluation of implant UWB-IR transmission with living animal for body area networks', *IEEE Trans. Microw. Theory Tech.*, 2014, **62**, (1), pp. 183–192
6 ICNIRP, 'Guidelines for limiting exposure to time varying electric magnetic and electromagnetic files (up to 300 GHz)', *Health Phys.*, 2009, **74**, pp. 494–522
7 Gao, S., Luo, Q., Zhu, F.: 'Circular polarized antennas' (Wiley-IEEE, 2014)
8 Morimoto, Y., Anzai, D., Wang, J.: 'Design of ultra wide-band low-band implant antennas for capsule endoscope application'. Proc. 7th Int. Symp. on Medical Information and Communication Technology (ISMICT), Tokyo, Japan, March 2013, pp. 61–64
9 Taflove, A., Hagness, S.C.: 'Computational electrodynamics: the finite-difference time-domain method' (Artech House, 2000, second edition)
10 Dissanayake, T., Yuce, R., Ho, C.: 'Design and evaluation of a compact antenna for implant-to-air UWB communication', *IEEE Antennas Wirel. Propag. Lett.*, 2009, **8**, pp. 153–156
11 Wang, Q., Wolf, K., Plettemeier, D.: 'An UWB capsule endoscope antenna design for biomedical communications'. Proc. Third Int. Application Science Biomedical Communication Technology Symp., (CD-ROM), Rome, Italy, November 2010
12 Yazdandoost, K.Y.: 'UWB antenna for body implanted applications'. Proc. 42nd European Microwave Conf., Amsterdam, The Netherlands, October 2012, pp. 932–935
13 Koshiji, F., Eguchi, T., Sato, K., Koshiji, K.: 'Proposal and investigation of unbalanced dipole antenna with semicircular and trapezoidal radiators for UWB radio', *J. Jpn Inst. Electron. Packag.*, 2007, **10**, (3), pp. 200–211
14 Nagaoka, T., Watanabe, S., Saurai, K., *et al.*: 'Development of realistic high-resolution whole-body voxel models of Japanese adult males and females of average height and weight, and application of models to radio-frequency electromagnetic-field dosimetry', *Phys. Med. Biol.* 2004, **49**, (1), pp. 1–15
15 Katsu, K., Anzai, D., Wang, J.: 'Performance evaluation on correlation detection and energy detection for ultra wideband-impulse radio communication with multi-pulse position modulation scheme in implant body area networks', *IET Commun.*, 2013, **7**, (13), pp. 1430–1436
16 Humblet, P.A., Azizoglu, M.: 'On the bit error rate of lightwave systems with optical amplifiers', *J. Lightw. Technol.*, 1991, **9**, (11), pp. 1576–1582
17 Proakis, J.G., Salehi, M.: 'Digital communications' (McGraw-Hill, 2008)
18 Wang, Q., Wang, J.: 'SA and SAR analysis for wearable UWB body area applications', *IEICE Trans. Commun.*, 2009, **E92-B**, (2), pp. 425–430